Geophysical Research Letters

RESEARCH LETTER
10.1029/2019GL083152

Influence of the QBO on the MJO During Coupled Model Multiweek Forecasts

S. Abhik[1] and Harry H. Hendon[1]

[1]Bureau of Meteorology, Melbourne, Victoria, Australia

Key Points:
- MJO amplitude is strengthened during coupled model forecasts that are initialized during austral summer when QBO is in its easterly phase
- MJO is promoted by enhanced tropopause destabilization during QBO easterly phase, and this effect is captured in the initialized forecasts
- Reduction of tropopause static stability is more in-phase with MJO convection during QBO easterly phase, promoting stronger MJO events

Supporting Information:
- Supporting Information S1

Correspondence to:
S. Abhik,
abhik.climate@gmail.com;
abhik.santra@bom.gov.au

Citation:
Abhik, S., & Hendon, H. H. (2019). Influence of the QBO on the MJO during coupled model multiweek forecasts. *Geophysical Research Letters*, *46*, 9213–9221. https://doi.org/10.1029/2019GL083152

Received 3 APR 2019
Accepted 10 JUN 2019
Accepted article online 18 JUN 2019
Published online 7 AUG 2019

Abstract Seasonal activity of the Madden-Julian Oscillation (MJO) is observed to be greater during austral summer when the lower stratospheric winds are in the easterly phase of the quasi-biennial oscillation (QBO). Using initialized predictions from two coupled model seasonal prediction systems, we show a systematic impact of the QBO on the amplitude of the MJO during the first few days of the forecast before model biases become too large. In both models as for the observed, the difference in MJO amplitude between easterly phases and westerly phases of the QBO increases with lead time, despite having similar initial amplitudes. Enhanced destabilization of the tropopause is argued to be the key mechanism that promotes stronger MJO convection during easterly phase of QBO. Caveats for the inability of the models to reproduce the observed strength of the MJO-QBO relationship are discussed.

Plain Language Summary The austral summertime Madden-Julian Oscillation (MJO) is observed to be stronger and more predictable when stratospheric winds are in the easterly phase of the quasi-biennial oscillation (QBO). The observed relationship between stratospheric QBO and MJO is examined in the multiweek forecasts from two ocean-atmosphere coupled models. A systematic impact of the QBO on the amplitude of the MJO is detected during the first few days of forecast. The predicted MJO with similar initial amplitude maintains its amplitude longer in the easterly phase of the QBO, while it weakens faster in the westerly phase of the QBO. We show that more in-phase reduction of tropopause static stability with the MJO convective anomalies during easterly phase of QBO promotes stronger MJO events, especially over the eastern side of the Maritime Continent. The predicted MJO during easterly phase of QBO is found to be stronger and propagates farther into the western Pacific.

1. Introduction

A significant and strong relationship between the Madden-Julian Oscillation (MJO) and the stratospheric quasi-biennial oscillation (QBO) has recently been discovered (Nishimoto & Yoden, 2017; Son et al., 2017; Yoo & Son, 2016). During the austral summer, seasonal mean MJO activity is enhanced when the equatorial lower stratospheric winds are in the easterly phase of the QBO (hereafter QBOE) and decreased during the westerly phase of the QBO (hereafter QBOW). Moreover, during QBOE, stronger MJOs propagate farther into the western Pacific (Nishimoto & Yoden, 2017; Son et al., 2017) and they are more predictable (Lim et al., 2019; Marshall et al., 2017).

Although the impact of the QBO on the MJO is well established, the mechanism of the impact is still uncertain. Hendon and Abhik (2018) proposed that a combination of MJO- and QBO-induced reductions in static stability at the tropopause plays an important role in strengthening MJO convection during QBOE. The QBO easterlies in the lower stratosphere overlay colder temperatures down to the tropopause in order to maintain thermal wind balance (Son et al., 2017). Hence, QBOE is associated with a destabilized equatorial tropopause region. Additionally, MJO convection adiabatically induces an overriding cold cap anomaly at and above the tropopause. The MJO-induced cold cap anomaly above active convection acts to further destabilize the tropopause region in addition to that produced during QBOE, thus promoting stronger MJO convection during QBOE. This destabilization strengthens convection more in phase with the MJO-induced temperature anomaly, thus acting to promote a stronger MJO.

Some support for this proposed mechanism to strengthen convection by destabilization of the tropopause region during QBOE is provided by idealized model studies that impose QBO temperature anomalies at the tropopause (Martin et al., 2019; Nie & Sobel, 2015). These studies find that convection is deepened in

response to imposed QBOE temperature profile (i.e., an anomalously cold tropopause). However, the models used in these studies (e.g., limited domain cloud resolving models) do not support a self-generated MJO and there is no two-way feedback to the outer domain. So, it is not yet clear how applicable their results are to the observed MJO-QBO interaction. There is no evidence yet of an impact of the QBO on the MJO in more comprehensive global models that support both the QBO and the MJO. For instance, Lee and Klingaman (2018), using long free runs of a version of the United Kingdom Meteorological Office (UKMO) climate model that has both a well resolved stratosphere (that supports QBO) and an improved depiction of the MJO, were unable to detect an impact of the QBO on the simulated MJO. They note, however, that biases in the vertical structure of both the simulated QBO and MJO may have prevented the interaction.

Here we take an alternative approach and use initialized coupled model multiweek predictions to explore the impact of the QBO on the MJO. As the forecasts are initialized with realistic depictions of both the QBO and the MJO, an impact of the QBO on the MJO might be felt in the first few days of the forecast before the model has drifted too far away from the reality. We explore this premise using two coupled model prediction systems. Both are initialized using best guesses of the observed atmosphere-ocean states, and both perform well in predicting the MJO to lead times of at least 3 weeks. One of the models has a well-resolved stratosphere and maintains the QBO for many days, whereas the other model has a low top and poor resolution in the stratosphere and the QBO weakens by about 50% at 3- to 4-week lead time. In order to maximize any impact of the QBO, we will concentrate on behavior of the MJO in the first ~2-3 weeks of the forecasts.

2. Model Configurations and Methodology

One of the models that we use in this study is the Predictive Ocean Atmosphere Model for Australia version 2 (POAMA-2), the ocean-atmosphere coupled prediction system used operationally for seasonal prediction at the Australian Bureau of Meteorology (BoM) during 2011–2018. The atmospheric component of POAMA-2 has coarse resolution (~250-km horizontal resolution) and the model top is low (~9 hPa). In the hindcasts used here, the model's atmosphere is initialized by nudging to ERA-40 reanalyses (Hudson et al., 2011) and ocean initial conditions are provided by the PEODAS system (Yin et al., 2011), which uses an ensemble optimum interpolation of available subsurface temperature and salinity observations. POAMA-2's performance for predicting the MJO is well documented (e.g., Marshall et al., 2011), and it also well captures improved predictability of the MJO during QBOE (Marshall et al., 2017). For this study, we use reforecasts initialized on the 1st, 6th, 11th, 16th, 21st, and 26th of each month between December and February (DJF) during 1990–2012. Reforecasts extend to 9-month lead time, but we concentrate on MJO behavior in the first month. A 33-member ensemble is available, but we sample 11 members to be compatible with the other model used in this study.

We use another coupled prediction system, Australian Community Climate and Earth-System Simulator-Seasonal prediction system version 1 (ACCESS-S1; Hudson et al., 2017). It replaced the POAMA-2 operational seasonal forecasting system at the BoM in 2018. ACCESS-S1 is based on the UKMO Global Seasonal forecast system version 5, using the Global Coupled model configuration 2 (MacLachlan et al., 2015). The horizontal resolution of the atmospheric model is ~60 km, and it has 85 vertical levels with a well resolved stratosphere (35 levels above 18 km) that supports a QBO (e.g., Walters et al., 2017). The ocean model has 25-km horizontal resolution and 70 vertical levels (~1-m resolution in top 10 m). For the hindcasts used here, the atmospheric initial conditions are derived by interpolating ERA-Interim reanalysis (ERA-I; Dee et al., 2011) directly onto the model grid. The ocean initial conditions are obtained from the Forecast Ocean Assimilation Model analyses at the UKMO (Blockley et al., 2014), which is a 3-D variational assimilation of available temperature, salinity, and sea level observations. Reforecasts are available from the 1st, 9th, 17th, and 25th of each month during DJF 1990–2012. An 11-member ensemble is produced by perturbing the atmospheric initial conditions (Hudson et al., 2017).

The approach in this study is to examine the evolution of the amplitude of the MJO in the first month of the forecasts, stratifying by initialization during QBOE and QBOW. To account for increased amplitude of the MJO during QBOE, we further bin the forecasts by the initial strength of the MJO. This provides an opportunity to examine the MJO events with similar magnitude during QBOE and QBOW. We use three bins: weak, moderate, and strong (defined below). We then compare the evolution of the amplitude of the MJO during the forecasts, averaged across all the forecasts in each of these three bins.

The differences in the evolution of the MJO amplitude associated with QBO may arise because of some systematic differences in the occurrence of particular phases of the MJO between QBOE and QBOW. We explore this possibility by further binning the MJO events based on the three amplitude bins into eight MJO phases. Although further subdivision into eight phases reduces the sample sizes accordingly, we could not detect any systematic differences in occurrences of any of the MJO phases between QBOE and QBOW. Thus, all initial MJO phases are equally treated in this study.

We define the state of the QBO using an index formed by equatorially averaging (5°S to 5°N) ERA-I zonal mean zonal wind at 50 hPa. Following Hendon and Abhik (2018), QBOW and QBOE are defined when the seasonal mean (DJF) index is greater than 0.5 standard deviations and less than −0.5 standard deviations, respectively. Out of a total 23 years of hindcast period (1990–2012), 7 austral summer seasons are classified as QBOE and 11 are classified as QBOW (years are provided in supporting information Table S1).

Although earlier studies (e.g., Nishimoto & Yoden, 2017) revealed a limited impact of El Niño–Southern Oscillation (ENSO) on the QBO-MJO interaction, primarily because ENSO does not strongly impact MJO activity on seasonal timescales during boreal winter (Hendon et al., 1999, 2007), a possible impact of ENSO on the evolution of MJO amplitude might not be excluded. Our prime concern is an apparent tendency to have more La Niña events during QBOE. To avoid any bias toward La Niña in QBOE, we reproduce our key results after removing strong ENSO years. We identify El Niño and La Niña years using the Oceanic Niño Index (ONI), which is based on 3-month running mean anomaly of the Niño-3.4 sea surface temperature index. The years of strong El Niño or La Niña are defined when the ONI during DJF is greater than 0.75 or less than −0.75, respectively. The QBOE and QBOW years that coincide with strong ENSO years, along with their corresponding ONI values, are indicated in supporting information Table S1.

We monitor the MJO using the pair of Real-time Multivariate MJO (RMM) indices (Wheeler & Hendon, 2004). The observed indices are derived by projecting equatorially averaged (15°S to 15°N) anomalies of daily top-of-the atmosphere outgoing longwave radiation (OLR; Liebmann & Smith, 1996) and zonal winds at 850 and 200 hPa from ERA-I onto the leading pair of observed empirical orthogonal functions (Wheeler & Hendon, 2004). Similarly, the predicted RMM indices for each ensemble member are computed by projecting the predicted equatorially averaged OLR and zonal wind anomalies onto the same pair of the observed empirical orthogonal functions. The predicted anomalies are formed using lead-time- and start-time-dependent model climatology for 1990–2012. Before projecting the forecast anomalies onto the observed eigenvector, the previous 120-day mean, which is a combination of observed and forecast data, are subtracted from each field following the approach of Rashid et al. (2011).

The daily MJO amplitude (observed and predicted) is defined as

$$|RMM(t)| = \sqrt{RMM_1^2(t) + RMM_2^2(t)}$$

We group the forecasts by start times occurring during QBOE and QBOW. Forecasts of the RMM are verified using bivariate correlation and root-mean-square error as described in Rashid et al. (2011). In order to examine the impacts on the MJO events with similar amplitude during QBOE and QBOW, we bin the forecasts by the amplitude of the observed MJO at the initial time $t = 0$ according to $|RMM(0)| < 1.0$ (weak), $1.0 \leq |RMM(0)| \leq 1.5$ (moderate) and $|RMM(0)| > 1.5$ (strong). The mean initial amplitudes during QBOE and QBOW for each of the three bins are nearly identical. Using more bins might help to make the initial amplitudes more similar, but this is at the expense of smaller numbers, hence, noisier results. Tweaking the boundaries of the three bins can also make the amplitudes during QBOE and QBOW more similar for one or two of the bins, but it can also make the mean amplitude difference between QBOE and QBOW even larger for the remaining bins. Our choice of the 3 bins used here seems to be a good compromise. However, our results are not sensitive to the choice of bin boundaries.

3. Impact of QBO on MJO During the Forecasts

We first examine the depiction of the QBO in both the models. We concentrate on the temperature structure in the lower stratosphere/tropopause region because previous modeling studies (e.g., Martin et al., 2019) and observational analysis (Hendon & Abhik, 2018; Klotzbach et al., 2019) point to QBO-temperature changes there as being the driver of changes in MJO behavior. The zonal mean temperature differences between QBOE and QBOW during DJF are displayed using ERA-I (Figure 1a) and using the first 10 days of forecasts

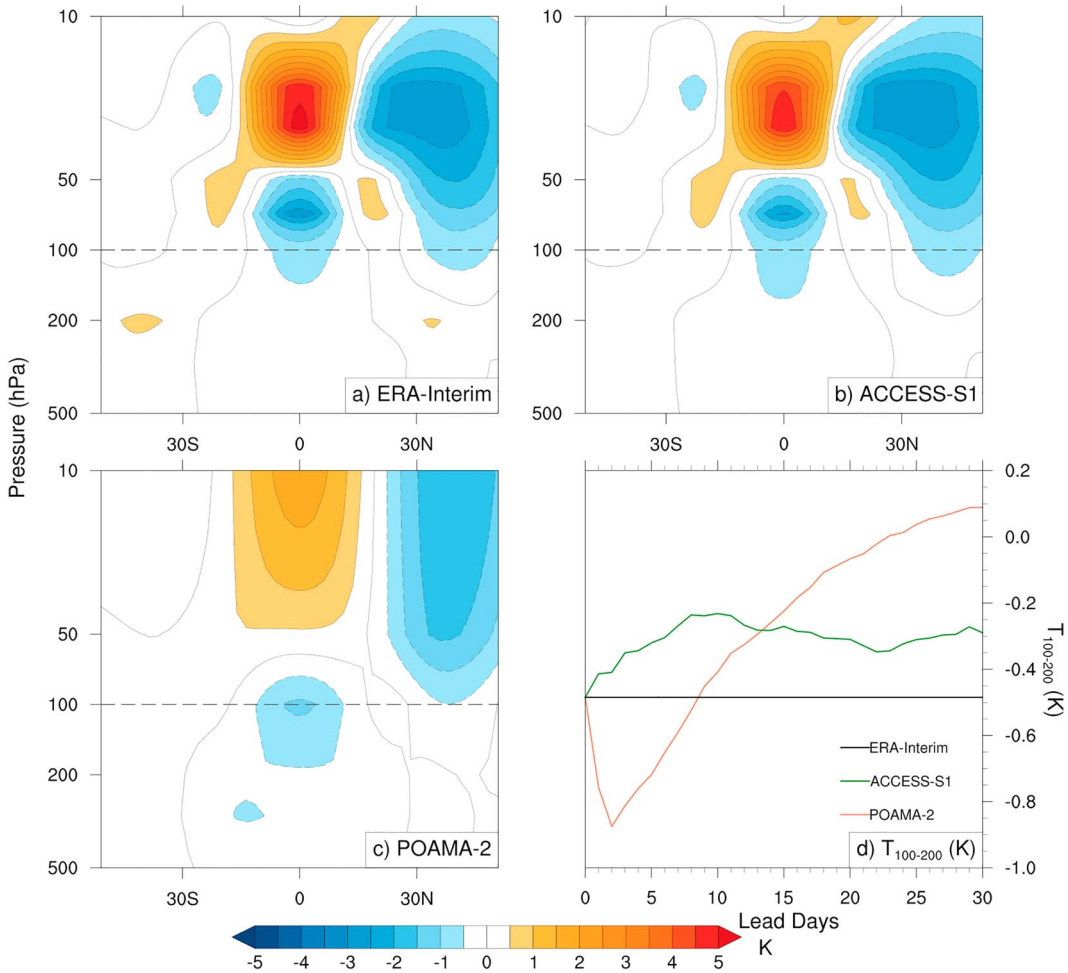

Figure 1. Zonal mean temperature difference between QBOE and QBOW during December-February for (a) ERA-Interim and for the mean of the first 10 days of forecasts initialized on December–February start dates from (b) ACCESS-S1 and (c) POAMA-2 during 1990 and 2012. (d) The daily lead-time evolution of the mean difference between QBOE and QBOW for the tropopause stability (defined as the temperature difference between 100 and 200 hPa) for ERA-Interim (black), ACCESS-S1 (green), and POAMA-2 (orange). Zonal mean of the mean tropopause stability difference is averaged over 5°S to 5°N. QBO = quasi-biennial oscillation; QBOE = easterly phase of the QBO; QBOW = westerly phase of the QBO; POAMA-2 = Predictive Ocean Atmosphere Model for Australia version 2; ACCESS-S1 = Australian Community Climate and Earth-System Simulator-Seasonal prediction system version 1.

from ACCESS-S1 (Figure 1b) and POAMA-2 (Figure 1c). These difference plots are indicative of the easterly phase of the QBO. The observed temperature anomaly for QBOE is characterized by an equatorially confined cold anomaly that is centered at about 70 hPa and extends downward to the tropopause level, reflecting thermal wind balance associated with peak QBO easterlies that are centered at about 50 hPa (not shown). The overlaying warm anomaly centered at about 30 hPa is associated with next descending westerly phase of the QBO. The off-equatorial temperature anomalies are understood as a response to induced changes in meridional circulation and extratropical eddy momentum flux divergence (Garfinkel et al., 2012). The depiction of the equatorial lower stratosphere/tropopause temperature anomaly appears to be well depicted in the ACCESS-S1 forecasts, reflecting the model's well-resolved stratosphere and capability to maintain and support the QBO. POAMA-2, however, has a much weaker and more vertically diffused equatorial temperature anomaly, reflecting the model's low stratospheric resolution and lack of parameterized gravity wave forcing to maintain the QBO. Nonetheless, at the tropopause level, POAMA-2 displays a similar magnitude of equatorial cold anomaly as observed.

The QBO-temperature change around the tropopause is quantified by considering the lead-time evolution of the mean temperature difference between 100 and 200 hPa (T_{100}-T_{200}) averaged zonally and between 5°S

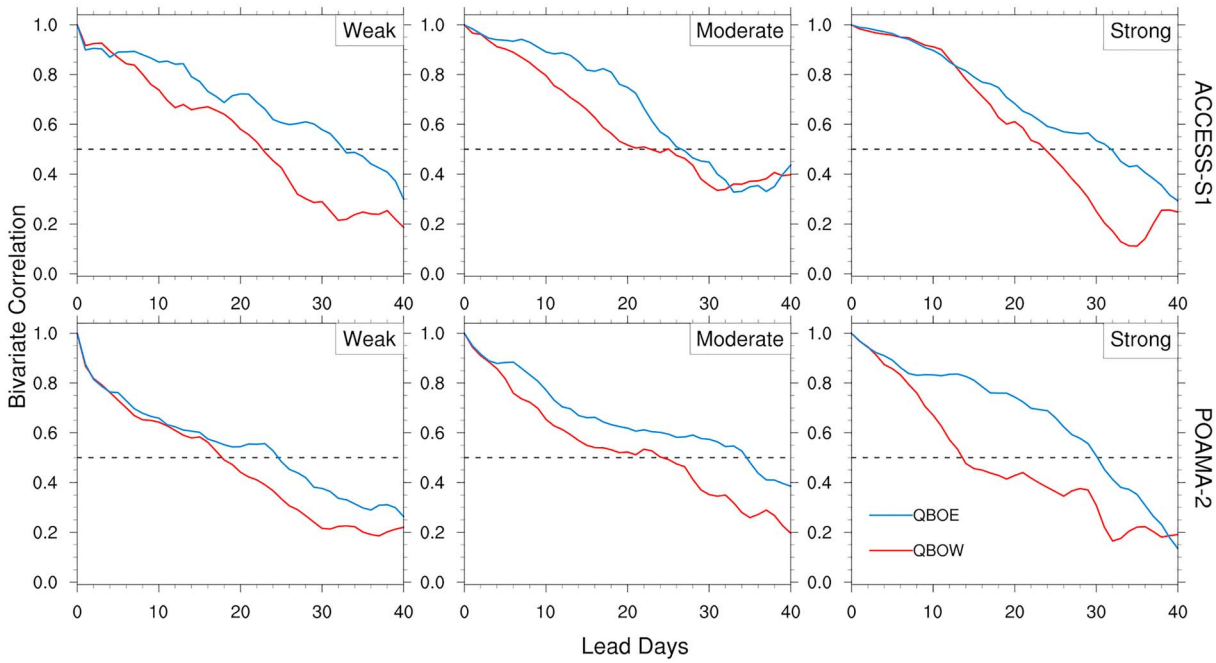

Figure 2. RMM bivariate correlation using ensemble mean from ACCESS-S1 (top panels) and POAMA-2 (bottom panels). Forecasts are initialized during the easterly phase of the QBO (blue solid) and westerly phase of the QBO (red solid) for start times in December–February 1990–2012. Subsets are based on (left) weak MJO amplitude ($|RMM(0)| < 1.0$), (middle) moderate amplitude ($1.0 \leq |RMM(0)| \leq 1.5$), and (right) strong amplitude ($|RMM(0)| > 1.5$) at the initial time. MJO = Madden-Julian Oscillation; RMM = Real-time Multivariate MJO; POAMA-2 = Predictive Ocean Atmosphere Model for Australia version 2; ACCESS-S1 = Australian Community Climate and Earth-System Simulator-Seasonal prediction system version 1; QBO = quasi-biennial oscillation.

and 5°N from the two models and observation (Figure 1d). The decreased tropopause stability during QBOE in ACCESS-S1 adjusts to about 50% of the observed value in ∼5 days, which is then maintained to 30-day lead time (and beyond). POAMA-2, however, shows rapid adjustment in the first 3–4 days, with the stability reduction becoming greater then observed, but it then asymptotes toward zero with increasing lead time, reflecting lack of the QBO signal in the model. Nonetheless, for the first ∼15 days, the mean reduction in stability during QBOE is similar in both the models. Therefore, it is feasible that the QBO could affect the MJO in POAMA-2 as much as it does in ACCESS-S1, at least in the first couple of weeks of the forecast before the depiction of the QBO is more severely degraded.

We next confirm that both ACCESS-S1 and POAMA-2 exhibit enhanced MJO prediction skill when initialized during QBOE. Although forecast skill of the MJO is not necessarily a prerequisite for producing an impact of the QBO on the MJO, it does provide some confidence that the MJO is realistically maintained during the forecasts. To account for possible impacts of enhanced MJO amplitude on enhanced prediction skill during QBOE, we assess forecast skill based on the three bins of initial MJO amplitude (weak, moderate, and strong). For the available ACCESS-S1 hindcast set used here, there are 21, 18, and 45 initial start times for weak, moderate, and strong cases, respectively, during QBOE. Similarly, there are 56, 36, and 40 initial start times for weak, moderate, and strong cases, respectively, during QBOW. For POAMA-2, 42 (104), 38 (54), and 46(40) initial start times are accounted for weak, moderate, and strong cases, respectively, during QBOE (QBOW).

The bivariate correlation for the RMM indices, binned for QBOE and QBOW and by initial MJO amplitude is displayed in Figure 2. Similarly, the normalized bivariate root-mean-square error for the RMM indices is displayed in Figure S1. Forecast skill from both ACCESS-S1 and POAMA-2 is systematically higher during QBOE, regardless of the initial amplitude of the MJO, which confirms the findings of Marshall et al. (2017) and Lim et al. (2019). When all forecasts are considered regardless of initial amplitude (Figure S2), the skill from POAMA-2 and from ACCESS-S1 is similar during QBOE (i.e., bivariate correlation drops to 0.5 at about 32-day lead time), but the drop in skill during QBOW is greater in POAMA-2 than in ACCESS-S1; that is, correlation drops to 0.5 at about 18 days in POAMA-2 but at about 22 days in ACCESS-S1. However, the cause of this greater drop in skill during QBOW in POAMA-2 is not clear.

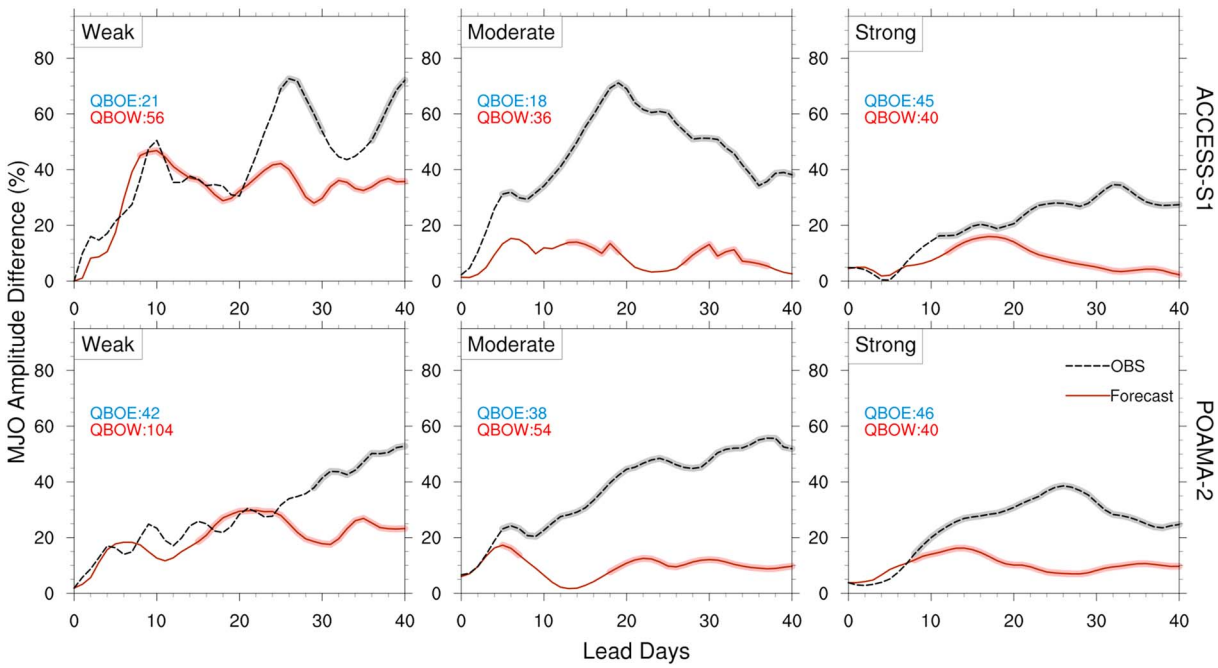

Figure 3. Mean RMM percentage amplitude difference between QBOE and QBOW computed using individual ensemble members from ACCESS-S1 (solid curve top panels) and POAMA-2 (solid curve bottom panels). The observed mean amplitude difference is dashed. Differences significantly different from zero at 5% level (see text) are highlighted in light brown (forecasts) and gray (observed). Three subsets are based on (left) weak MJO amplitude ($|RMM(0)| < 1.0$), (middle) moderate amplitude ($1.0 \leq |RMM(0)| \leq 1.5$), and (right) strong amplitude ($|RMM(0)| > 1.5$) at the initial time. The number of start times in each QBO phase is indicated in top left (blue for QBOE and red for QBOW). MJO = Madden-Julian Oscillation; RMM = Real-time Multivariate MJO; POAMA-2 = Predictive Ocean Atmosphere Model for Australia version 2; ACCESS-S1 = Australian Community Climate and Earth-System Simulator-Seasonal prediction system version 1; QBO = quasi-biennial oscillation; QBOE = easterly phase of the QBO; QBOW = westerly phase of the QBO.

We now turn to the impact of the QBO on the amplitude of the MJO during the forecasts. If the MJO realistically "feels" the QBO during the forecast, then we would expect the amplitude to increase more (in the case of initialized with weak amplitude) or decrease less (in the case of initialized with strong amplitude) during QBOE compared to QBOW. This is confirmed in Figure 3, which shows the time evolution of the mean percentage difference of MJO amplitude between QBOE and QBOW when binned by similar initial amplitude. Although there is evidence of systematically larger initial amplitude during QBOE for some of the bins, this initial amplitude difference is small relative to the differences that develop at longer lead times. Here we use individual ensemble members to compute the amplitude, such that we are treating the forecast outputs in the same fashion as the single sample from reality. The difference is shown both for forecasts (as function of lead time) and from observations. The evolution of the actual mean amplitudes for each of the cases are shown in Figure S3. In observations and forecasts, greater amplitude develops during QBOE, despite nearly identical mean amplitude at the initial time for each of the three bins. We also infer from Figure S3 that the mean RMM amplitude is larger in POAMA-2 compared to ACCESS-S1, which is consistent with the finding of Marshall and Hendon (2019) that the simulated MJO is slightly stronger than observed in POAMA-2 and weaker than observed in ACCESS-S1.

Statistically significant differences in amplitude are also highlighted in Figure 3. Generally, the difference in MJO amplitude between QBOE and QBOW becomes significant after ~5 days from the start day. The significance is estimated using a t test assuming a null hypothesis of no difference. For the observed differences, the sample sizes are the number of cases during QBOE and QBOW in each bin. We account for the 11 ensemble members of the forecasts but reduce the effective sample size by considering the lead-time dependent correlation of the members (Bretherton et al., 1999)

$$N_{eff} = N\frac{1-r^2}{1+r^2}.$$

Here, N is the total sample size (= all start times in each bin ×11 ensemble members) and r is the mean correlation of each member with all other ensemble members at each lead time. This correlation coefficient

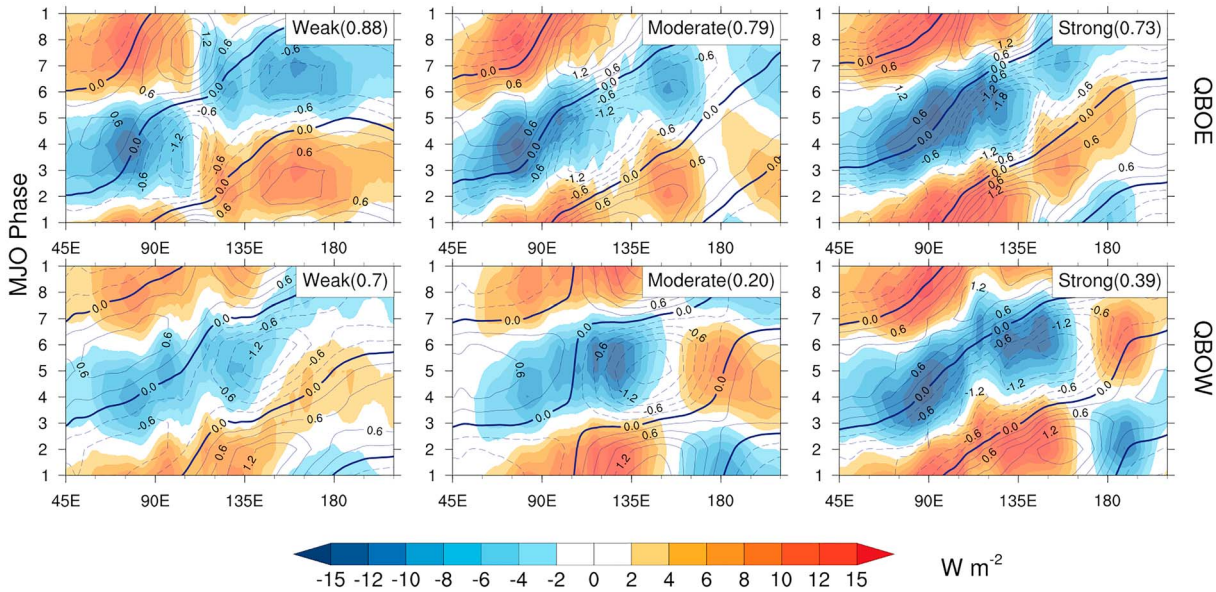

Figure 4. Equatorially averaged anomalies of OLR (shaded, W/m^2) and tropopause stability (contours, K) regressed onto the ensemble mean RMM indices using days 5–12 of the forecast from ACCESS-S1. The top row is during QBOE, and bottom row is during QBOW. Regressions are formed separately for weak (left column), moderate (middle), and strong (right) initial RMM amplitudes. Regression coefficients are scaled for a one standard deviation anomaly of the RMM indices. The correlation between tropopause stability and OLR anomalies computed across all MJO phases at each longitude and then averaged over 90°E to 180° is mentioned in top right of each panel. OLR = outgoing longwave radiation; MJO = Madden-Julian Oscillation; RMM = Real-time Multivariate MJO; ACCESS-S1 = Australian Community Climate and Earth System Simulator-Seasonal prediction system version 1; QBOE = easterly phase of the QBO; QBOW = westerly phase of the QBO; QBO = quasi-biennial oscillation;

r is equivalent to the potential predictability and monotonically decreases from greater than 0.9 at shortest lead time to about 0.6 at lead time 30 days. We apply a 3-day running mean on the amplitude differences across the lead time for smoothing.

In both models, the weaker difference in MJO amplitude between QBOE and QBOW that develops during the forecast compared to the observed difference may stem from biases in the model's MJO and QBO. As shown in Figure 1d, the QBO's impact on equatorial tropopause stability is weaker than observed for both models after the first ~10 days of the forecast. This would weaken the destabilization around the tropopause, which is hypothesized to enhance the MJO during QBOE. ACCESS-S1 does maintain the QBO signal at the tropopause longer into the forecast, but the predicted MJO is weaker than observed, especially in the western Pacific (e.g., Marshall & Hendon, 2019). POAMA-2 simulates a stronger than observed MJO (Marshall et al., 2011), but it also has weaker than observed convective anomalies as the MJO propagates into the western Pacific. Nonetheless, both models show a consistent enhanced MJO amplitude during the forecasts independent of the initial amplitude. This suggests that the models' MJO are "feeling" the QBO.

In order to assess a possible influence from ENSO on the change in amplitude of the MJO during the forecasts, we recompute the calculation for Figure 3 by excluding the strong ENSO years (Figure S4). As indicated in supporting information Table S1, we exclude three (1998–1999, 2005–2006, and 2007–2008) DJF seasons from QBOE and six (1995–1996, 1997–1998, 1999–2000, 2002–2003, 2008–2009, and 2009–2010) DJF seasons from QBOW. The same general behavior as seen in Figure 3 is reproduced in Figure S4. This confirms that the enhanced growth of MJO amplitude during QBOE is unlikely a result of the MJO preferentially growing more during La Niña events, which apparently occur more often during QBOE.

Hendon and Abhik (2018) argued that if the QBO is affecting the MJO, making it stronger during QBOE, then the vertical structure of the MJO ought to be different during QBOE compared to QBOW. We assess this difference in vertical structure by forming the composite structure of the OLR and tropopause stability anomalies during QBOE and QBOW for weak, moderate, and strong MJO amplitude cases at the initial time. To focus on the MJO after it begins to feel the QBO during the forecasts, we use forecast output from days 5–12 (results are not sensitive to these limits). The tropopause stability anomaly is defined as the anomalous temperature difference between 100 and 200 hPa ($T_{100} - T_{200}$). Following a similar approach as Virts and Wallace (2014), we form the composite by regression onto the time series of

$RMM_1(t)$, $RMM_1(t) + RMM_2(t)$, $RMM_2(t)$, and $RMM_2(t) - RMM_1(t)$, which gives anomalies indicative of the Wheeler and Hendon (2004) MJO phases 4/5, 5/6, 6/7, and 7/8, respectively. The other four phases are obtained by simply reversing the sign of the anomalies in these four phases. For display, the regressed anomalies are scaled by one standard deviation of the corresponding RMM indices. The regressions are done separately for QBOE and QBOW and for weak, moderate, and strong initial observed MJO amplitudes. In Figure 4, we display the regressed tropopause stability and OLR anomalies along the equator as a function of 8 MJO phases using 5- to 12-day forecasts from ACCESS-S1. Similar plots are shown in Figure S5 using POAMA-2 forecasts and in Figure S6 for observation. For observation, we use days 5–12 after the key dates are identified at the initial time. For both models and observed, eastward propagation of MJO convection is depicted, which is stronger in cases with initially greater MJO amplitude. However, the convective anomaly propagates farther into the western Pacific during QBOE especially for the moderate and strong cases. Both the models reasonably reproduce the observed MJO characteristics but neither of them show MJO propagation as far into the western Pacific as observed.

The observed and forecasted tropopause temperature anomalies are seen to be largely in quadrature with the OLR anomaly, which would be expected if the MJO behaved as a propagating Kelvin wave. However, the negative OLR anomaly is shifted into the negative stability anomaly in the eastern Indian Ocean and West Pacific. Hendon and Abhik (2018) interpreted this shift as an indication of a positive feedback between temperature and convection: the more in-phase the OLR and stability anomalies, the stronger the feedback. The shift is more apparent during QBOE and the difference in phasing between QBOE and QBOW is more apparent in the ACCESS-S1. Following the approach of Hendon and Abhik (2018), the phasing of the OLR and stability anomalies is quantified by computing their correlation across the eight phases and at each longitude over 90°E to 180° and then averaging. The mean correlation is displayed in the upper right of each panel in Figures 4, S5, and S6. The observed correlations (Figure S6) are systematically more positive during QBOE for all three amplitude bins, consistent with the findings of Hendon and Abhik (2018) and this behavior is well depicted in both the models. This more in-phase relationship of anomalous convection with reduced tropopause stability during forecasts initialized during QBOE thus supports the notion that the model's MJO is realistically reacting to the additional destabilization provided during QBOE, thus producing a stronger MJO than during QBOW.

4. Discussion and Conclusions

We show a systematic impact of the QBO on the amplitude of the MJO using initialized predictions from two coupled model seasonal prediction systems. For the hindcasts initialized during the DJF seasons of 1990–2012, both models indicate that the MJO grows more (when initialized with weak MJO amplitude) or decays less (when initialized with strong MJO amplitude) during QBOE compared to QBOW. Although the change in amplitude of the predicted MJOs are weaker than the observed MJOs, the enhancement of MJO amplitude during forecasts initialized in QBOE is systematic across both the models and is not dependent on initial MJO amplitude or on the state of ENSO.

Promotion of stronger MJO amplitude during QBOE appears to result from amplified MJO-induced destabilization above the deep convection: during easterly phases of the QBO in the lower stratosphere, temperatures are cooler than normal down to the tropopause, which then get amplified by the MJO-induced reduction of stability above the regions of enhanced convection. This subsequently promotes enhanced convection that is more in-phase with the MJO temperature anomaly. This enhancement is found in both forecast models, despite different depictions of the QBO and the MJO in each model. The weaker than observed impact on amplitude of the MJO in both models presumably reflects model biases in both the depiction of the MJO and the QBO, but further study is required to illuminate which biases are more important. Our results do not preclude the possibility of stronger MJO activity during QBOE due to some other aspect of the QBO (e.g., changes in upper tropospheric wind shear, changes in cloud-radiative forcing). These will likely be subject to further investigation.

Lee and Klingaman (2018), who used a model similar to ACCESS-S1, were not able to detect an impact of the QBO on the MJO. In their study, they looked at the behavior of the MJO and QBO in long free runs of the model. The MJO and the QBO were purely generated by the model, and so biases in both the MJO and the QBO may have prevented detection of any impact. In contrast, the approach of the present study is to use initialized forecasts, so that at least early on the forecast, the MJO and QBO are more representa-

tive of reality, thus allowing an impact of the QBO on the MJO to be detected, albeit weaker impact than observed. However, even at short lead time, there are clear biases in the MJO and QBO in both models, and the impact of these biases is still unknown. To this end, the S2S database (Vitart et al., 2017), which is an archive of multiweek forecasts from several forecast models, could be explored to further assess the impact of the QBO on the amplitude of the MJO in the same way. Critical dependencies on model biases then might be revealed (e.g., the relative impact of a poor depiction of the QBO versus a poor depiction of the MJO), which might also guide improvement in the overall depiction and prediction of the MJO. Besides the variation of equatorial tropopause temperature, other aspects of the QBO (e.g., variations of upper tropospheric vertical and horizontal wind shear) could be responsible for modulating MJO amplitude and require further investigation.

Acknowledgments
SA acknowledges support from the Earth System and Climate Change Hub of the Australian Governments National Environmental Science Programme (NESP). We thank Andrew Marshall for providing RMM indices for POAMA-2. Suggestions from Rob Colman and constructive comments from two anonymous reviewers helped to improve the quality of the manuscript. ERA-Interim reanalysis were downloaded from ECMWF website (https://apps.ecmwf.int/datasets/data/interim_full_daily). Daily interpolated OLR data were obtained from NOAA/ESRL PSD, Boulder, Colorado, USA (https://www.esrl.noaa.gov/psd/data/gridded/data.interp_OLR.html). The ONI index is obtained from http://origin.cpc.ncep.noaa.gov/products/analysis_monitoring/ensostuff/ONI_v5.php website. This research was carried out with the assistance of resources and services from the National Computational Infrastructure (NCI) of Australian Government, and the analysis was performed using NCAR Command Language (NCL; https://doi.org/10.5065/D6WD3XH5).

References

Blockley, E., Martin, M., McLaren, A., Ryan, A., Waters, J., Lea, D., et al. (2014). Recent development of the Met Office operational ocean forecasting system: An overview and assessment of the new global FOAM forecasts. *Geoscientific Model Development*, *7*(6), 2613–2638.

Bretherton, C. S., Widmann, M., Dymnikov, V. P., Wallace, J. M., & Bladé, I. (1999). The effective number of spatial degrees of freedom of a time-varying field. *Journal of Climate*, *12*(7), 1990–2009.

Dee, D. P., Uppala, S. M., Simmons, A., Berrisford, P., Poli, P., Kobayashi, S., et al. (2011). The ERA-Interim reanalysis: Configuration and performance of the data assimilation system. *Quarterly Journal of the Royal Meteorological Society*, *137*(656), 553–597.

Garfinkel, C. I., Feldstein, S. B., Waugh, D. W., Yoo, C., & Lee, S. (2012). Observed connection between stratospheric sudden warmings and the Madden-Julian oscillation. *Geophysical Research Letters*, *39*, L18807. https://doi.org/10.1029/2012GL053144

Hendon, H. H., & Abhik, S. (2018). Differences in vertical structure of the Madden-Julian oscillation associated with the quasi-biennial oscillation. *Geophysical Research Letters*, *45*, 4419–4428. https://doi.org/10.1029/2018GL077207

Hendon, H. H., Wheeler, M. C., & Zhang, C. (2007). Seasonal dependence of the MJO–ENSO relationship. *Journal of Climate*, *20*(3), 531–543.

Hendon, H. H., Zhang, C., & Glick, J. D. (1999). Interannual variation of the Madden–Julian Oscillation during austral summer. *Journal of Climate*, *12*(8), 2538–2550.

Hudson, D., Alves, O., Hendon, H. H., Lim, E.-P., Liu, G., Luo, J.-J., et al. (2017). ACCESS-S1: The new Bureau of Meteorology multi-week to seasonal prediction system. *Journal of Southern Hemisphere Earth Systems Science*, *67*(3), 132–159.

Hudson, D., Alves, O., Hendon, H. H., & Wang, G. (2011). The impact of atmospheric initialisation on seasonal prediction of tropical pacific SST. *Climate Dynamics*, *36*(5-6), 1155–1171.

Klotzbach, P., Abhik, S., Hendon, H., Bell, M., Lucas, C., Marshall, A., & Oliver, E. (2019). On the emerging relationship between the stratospheric quasi-biennial oscillation and the Madden-Julian oscillation. *Scientific Reports*, *9*(1), 2981.

Lee, J. C., & Klingaman, N. P. (2018). The effect of the quasi-biennial oscillation on the Madden-Julian oscillation in the Met Office unified model global ocean mixed layer configuration. *Atmospheric Science Letters*, *19*, e816.

Liebmann, B., & Smith, C. A. (1996). Description of a complete (interpolated) outgoing longwave radiation dataset. *Bulletin of the American Meteorological Society*, *77*(6), 1275–1277.

Lim, Y., Son, S.-W., Marshall, A. G., Hendon, H. H., & Seo, K.-H. (2019). Influence of the QBO on MJO prediction skill in the subseasonal-to-seasonal prediction models. *Climate Dynamics*, 1–15. https://doi.org/10.1007/s00382-019-04719-y

MacLachlan, C., Arribas, A., Peterson, K., Maidens, A., Fereday, D., Scaife, A., et al. (2015). Global seasonal forecast system version 5 (GloSea5): A high-resolution seasonal forecast system. *Quarterly Journal of the Royal Meteorological Society*, *141*(689), 1072–1084.

Marshall, A. G., & Hendon, H. H. (2019). Multi-week prediction of the Madden-Julian oscillation with ACCESS-S1. *Climate Dynamics*, *52*(5–6), 2513–2528. https://doi.org/10.1007/s00382-018-4272-6

Marshall, A. G., Hendon, H. H., Son, S.-W., & Lim, Y. (2017). Impact of the quasi-biennial oscillation on predictability of the Madden–Julian oscillation. *Climate Dynamics*, *49*(4), 1365–1377.

Marshall, A. G., Hudson, D., Wheeler, M. C., Hendon, H. H., & Alves, O. (2011). Assessing the simulation and prediction of rainfall associated with the MJO in the POAMA seasonal forecast system. *Climate Dynamics*, *37*(11-12), 2129–2141.

Martin, Z., Wang, S., Nie, J., & Sobel, A. (2019). The impact of the QBO on MJO convection in cloud-resolving simulations. *Journal of Atmospheric Science*, *79*, 669–688.

Nie, J., & Sobel, A. H. (2015). Responses of tropical deep convection to the QBO: Cloud-resolving simulations. *Journal of Atmospheric Science*, *72*(9), 3625–3638.

Nishimoto, E., & Yoden, S. (2017). Influence of the stratospheric quasi-biennial oscillation on the Madden–Julian oscillation during austral summer. *Journal of Atmospheric Science*, *74*(4), 1105–1125.

Rashid, H. A., Hendon, H. H., Wheeler, M. C., & Alves, O. (2011). Prediction of the Madden-Julian oscillation with the POAMA dynamical prediction system. *Climate Dynamics*, *36*(3-4), 649–661.

Son, S.-W., Lim, Y., Yoo, C., Hendon, H. H., & Kim, J. (2017). Stratospheric control of the Madden–Julian oscillation. *Journal of Climate*, *30*(6), 1909–1922.

Virts, K. S., & Wallace, J. M. (2014). Observations of temperature, wind, cirrus, and trace gases in the tropical tropopause transition layer during the MJO. *Journal of Atmospheric Science*, *71*(3), 1143–1157.

Vitart, F., Ardilouze, C., Bonet, A., Brookshaw, A., Chen, M., Codorean, C., et al. (2017). The subseasonal to seasonal (S2S) prediction project database. *Bulletin of the American Meteorological Society*, *98*(1), 163–173.

Walters, D., Brooks, M., Boutle, I., Melvin, T., Stratton, R., Vosper, S., et al. (2017). The Met Office unified model global atmosphere 6.0/6.1 and JULES global land 6.0/6.1 configurations. *Geoscientific Model Development*, *10*(4), 1487–1520.

Wheeler, M. C., & Hendon, H. H. (2004). An all-season real-time multivariate MJO index: Development of an index for monitoring and prediction. *Monthly Weather Review*, *132*(8), 1917–1932.

Yin, Y., Alves, O., & Oke, P. R. (2011). An ensemble ocean data assimilation system for seasonal prediction. *Monthly Weather Review*, *139*(3), 786–808.

Yoo, C., & Son, S.-W. (2016). Modulation of the boreal wintertime Madden-Julian oscillation by the stratospheric quasi-biennial oscillation. *Geophysical Research Letters*, *43*, 1392–1398. https://doi.org/10.1002/2016GL067762